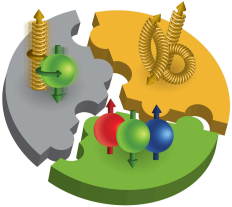

Absolute hadron beam polarimetry at EIC

Frank Rathmann

Community-wide meeting on
Polarized Ion Sources and Beams
Center for Frontiers in Nuclear Science, Stony Brook University
https://indico.cfnssbu.physics.sunysb.edu/event/343/
March 10, 2025

Contents I

Hadron polarimetry requirements for the EIC I

Comments

- The EIC will use polarized **protons** and **helions**, later on possibly deuterons, and heavier nuclei like lithium may be needed.
- **The EIC promises to provide proton beam polarizations of $P \geq 0.7$ with a relative uncertainty of $\Delta P/P \leq 1\%$.**
- Polarization calibration needed for each ion species as presently done:
  - elastic scattering of identical particles $\Rightarrow$ beam polarization inferred from known target polarization.
- **Absolute proton beam polarization calibration relies on precisely measured nuclear polarization of atomic jet using Breit-Rabi polarimeter.**

Hadron polarimetry requirements for the EIC II

Polarimeters shall determine:

- Bunch polarization profile in x, y, z
- Polarization lifetime
  - For EIC physics, projection of $\vec{P}$ on stable spin axis required, no in-plane polarization.
- Polarization vector $\vec{P}$ per bunch

Instruments

- Hadron polarimeter (absolute) in IP4
- pC polarimeter (relative) in IP4 and IP6 (between spin rotators)

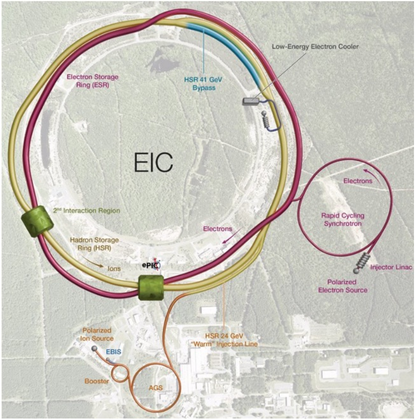

Asymmetry and polarization

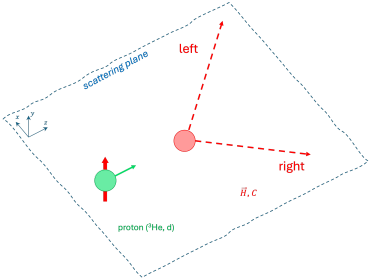

- Spin-dependent cross section

$$\sigma = \sigma_0(1 + A_y P_y \cos\phi) \quad (1)$$

  - Unpolarized cross section σ_0
  - P_y vertical component of beam polarization $\vec{P} = (P_x, P_y, P_z)$
  - Analyzing power $A_y = \frac{\sigma^{\text{left}} - \sigma^{\text{right}}}{\sigma^{\text{left}} + \sigma^{\text{right}}}$
  - Azimuth of scattered particle ϕ

Coulomb-nuclear interference (CNI) (see slide 62).)

- A_y: measure of polarization sensitivity of scattering process
- **At AGS and RHIC energies, no scattering processes available with A_y known to sufficient accuracy for $\Delta P/P \leq 0.01$ [1].**
- **Interference of EM and strong interaction at small scattering angles provides sizable analyzing power for elastic *pp* (and *pN*) scattering.**

Instruments for absolute and relative polarimetry

Two devices

- **HJET polarimeter**

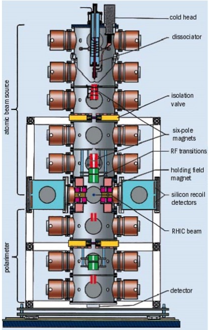

  - **absolute, slow**

$$\frac{\Delta P}{P} \approx 3\% \text{ per } 4 \text{ hour} \qquad (2)$$

- **pC polarimeters**

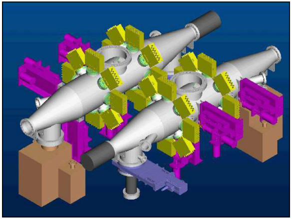

  - **fast, relative**
  - transverse profiles of polarization

$$\frac{\Delta P}{P} < 1\% \text{ per scan} \qquad (3)$$

Detector system at the polarized jet target

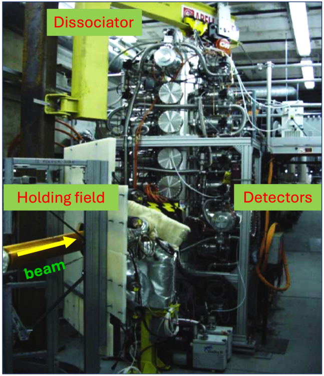

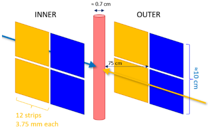

Eight Si strip detect.

- 12 vertical strips
- 3.75 mm pitch
- 500 μm thickness

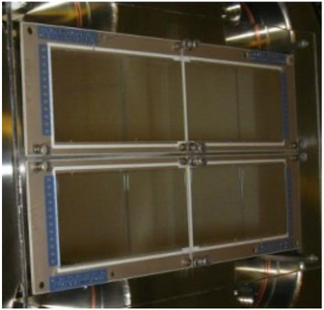

With present setup of L-R detectors and guide field B_y

- Only vertical component P_y measurable via L-R asymmetry near $\theta = 90^\circ$.

Absolute polarization from polarized hydrogen jet I

Breit-Rabi polarimeter

- Capable to determine absolute polarization Q of atomic beam, i.e., electron and proton polarization of hydrogen atoms, with accuracy $\Delta Q/Q \lesssim 1\%$.
    - Take this as a given. Will revisit subject through measurements after run 25.
    - No solid estimates available that fully encapsulate the BRP measurement systematics at the HJET on the $\approx 1\%$ level.

Beam polarization calibration

1. Proton beam passes through target of polarized H atoms of known polarization Q

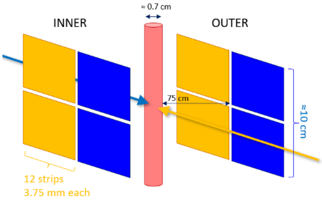

Absolute polarization from polarized hydrogen jet II

Beam polarization calibration

2. Measure number of scattered particles in left (L) and right (R) detectors
3. Sign of Q periodically reversed to compensate for asymmetries caused by differences in detector geometry or efficiency in L and R directions.
4. This determines target asymmetry
$$\epsilon_{\text{target}} = \frac{\text{L} - \text{R}}{\text{L} + \text{R}} = A_y \cdot Q \cos\phi\,. \tag{4}$$
5. Measurement of corresponding asymmetry with beam particles determines ϵ_{beam}. In elastic *pp* scattering, and more general in the elastic scattering of *identical* particles, A_y same regardless of which proton is polarized.
6. Absolute beam polarization given by
$$\boxed{P = \frac{\epsilon_{\text{beam}}}{\epsilon_{\text{target}}} \cdot Q} \tag{5}$$

Beam-induced target depolarization at RHIC and EIC

Polarized hydrogen jet

- Development of HJET for RHIC finished $\approx$ 20 yrs ago
  - Many technical details of design/development can't be found in literature
  - Designer just started to generate a 3D CAD model of HJET
  - There is no comprehensive publication on HJET available
- Grigori Atoian knows all that is needed to reliably operate the source
- Anatoli Zelenski is an excellent source of information
- Tom Wise gave me a bunch of write-ups and notes
- I am in touch with Alexander Nass
  - on BRP operation and last full polarization measurement (2004)
  - Alex gave me an unfinished paper draft

At EIC, beam current and bunch-repetition frequency much larger than at RHIC

- **Study beam-induced depolarization of target atoms**, and
- **How magnetic fields produced by beams in RHIC and EIC affect target polarization?**

Bunch structure

RHIC situation:

- Time period between two adjacent bunches: $\tau_\mathrm{b} = \frac{\tau_\mathrm{rev}}{N_b} = 106.57\,\mathrm{ns}$
- Number of stored bunches $N_b = 120$
- Bunch frequency $f_\mathrm{b} = \frac{1}{\tau_\mathrm{b}} = 9.3831\,\mathrm{MHz}$
- Large number of harmonics contribute to induced magnetic high-frequency field close to RHIC beam, as bunches are short ($\sigma_t \approx 1.8\,\mathrm{ns}$)

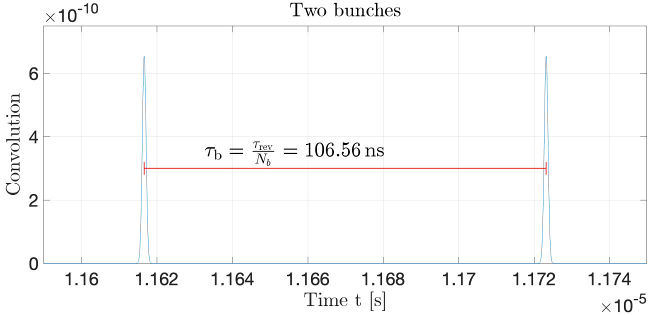

Hyperfine states of hydrogen

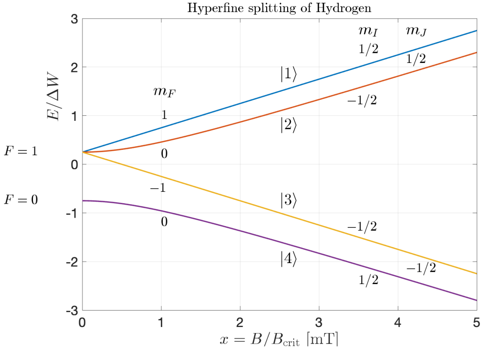

Critical field B_c (see slide 64)

- Zeeman energy $g_J \mu_B B$ comparable to E_{hfs}
- $E_{\mathrm{hfs}} \approx 5.874 \times 10^{-6}$ eV ($\approx$1420 MHz [2]):
- $B_c = 50.7\,\mathrm{mT}$

Transition frequencies

- between two hyperfine states $|i\rangle$ and $|j\rangle$ given by:

$$f_{ij} = \frac{E_{|i\rangle}(B) - E_{|j\rangle}(B)}{h} \tag{6}$$

- **When f_{ij} matches one of the beam harmonics at a certain holding field $|\vec{B}|$, resonant depolarization occurs [3]**

Single bunch distribution

- (Gaussian) bunch in RHIC

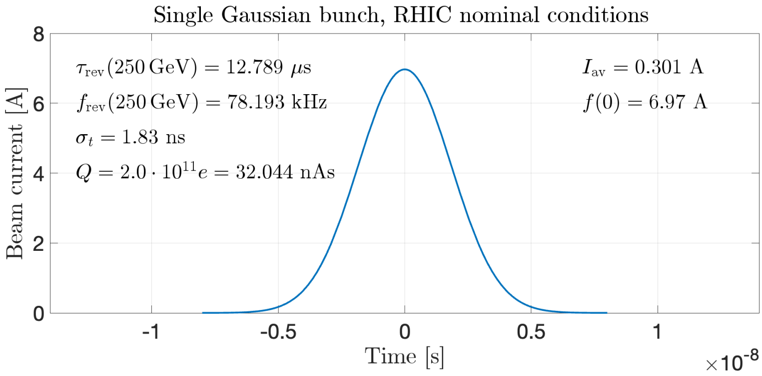

Pulse shape described by

$$f(t) = \frac{Q}{\sqrt{2\,\pi}\sigma_t} \exp\left(-\frac{t^2}{2\sigma_t^2}\right) \qquad (7)$$

Gaussian convoluted with (finite) series of delta functions

Total beam current as function of time t given by

$$I(t) = \int_{-\infty}^{\infty} f(t-\xi) \sum_{k=-\infty}^{\infty} \delta\left(\xi - k\frac{\tau_{\mathrm{rev}}}{N_{\mathrm{b}}}\right) \mathrm{d}\xi \qquad (8)$$

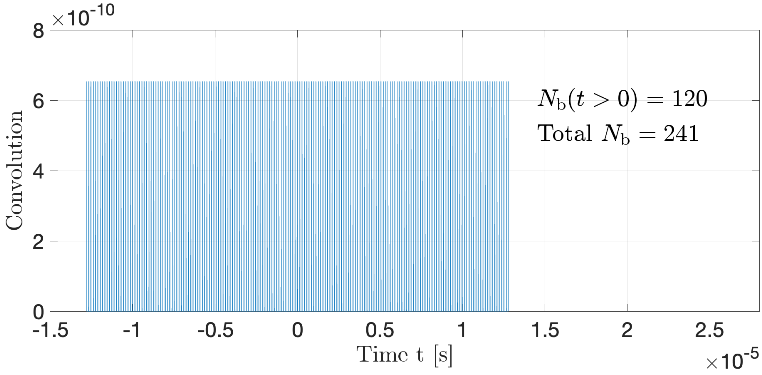

Produced radio-frequency fields from FFT of convolution

- Single-sided amplitude spectrum of FFT
- x-axis converted to frequency

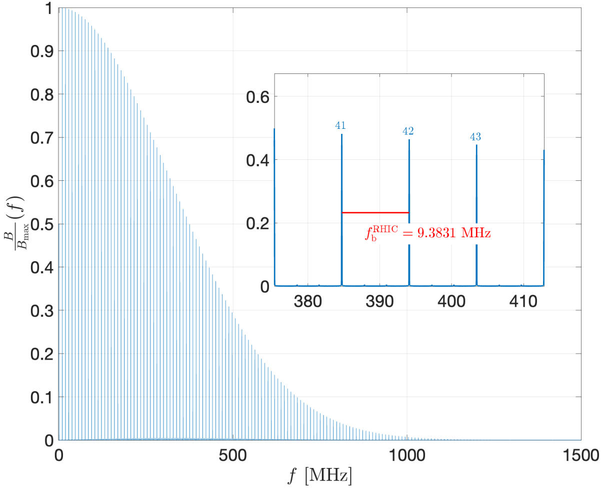

Transition frequencies between hyperfine states of H

Based on Zeeman splitting (slide 12) using Eq. (6)

- Determine transition frequencies f_{ij} between hyperfine states $|i\rangle$ and $|j\rangle$.
- Classification refers to change of quantum numbers (see Ramsey [4]):
  - B_0 is static field, B_1 is RF field that exerts torque on magnetic moment μ:
  - π ($B_1 \perp B_0$) transitions *within one F* multiplet:

$$\Delta F = 0, \quad \Delta m_F = \pm 1. \tag{9}$$

  - σ ($B_1 \parallel B_0$) transitions *between different F* multiplets:

$$\Delta F = \pm 1, \quad \Delta m_F = 0, \pm 1. \tag{10}$$

Possible transitions

- Single photon transitions in H: f_{12}^{π}, f_{23}^{π}, f_{14}^{σ}, f_{24}^{σ}, and f_{34}^{σ}.
- Transition $f_{13}^{2\gamma}$ with $\Delta m_F = 2$ requires two photons.

Transition frequencies between hyperfine states of H

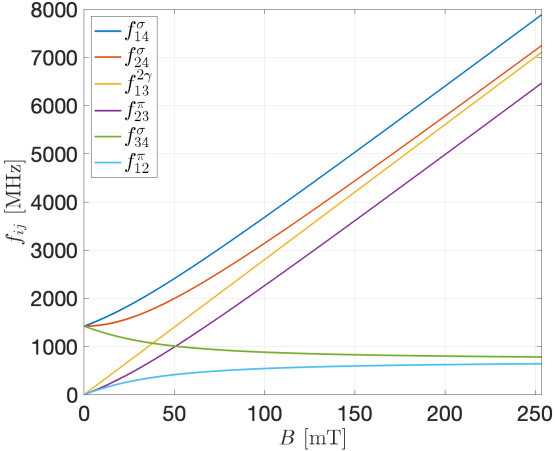

For $n = 4$ hyperfine states, $\binom{n}{2} = 6$ transitions possible.

Hyperfine transitions in H from bunch fields at RHIC

Depolarization occurs when f_{ij} multiple of bunch frequency f_b^{RHIC}

- HJET injects states $|1\rangle + |4\rangle$ ($p^{\uparrow}$) and $|2\rangle + |3\rangle$ ($p^{\downarrow}$).
  - What is exact magnitude and orientation of $\vec{B}^{\mathrm{HJET}}$? **Visit issue after run 25**

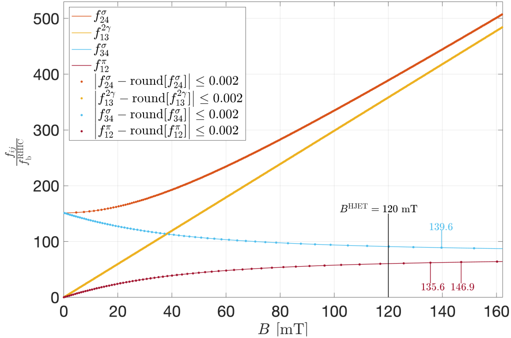

- $\left|\frac{f_{ij}}{f_b^{\mathrm{RHIC}}} - n\right| \leq 0.002\,,\ n \in \mathbb{N}$
- No depolarization from same $m_I \Rightarrow f_{14}^{\sigma}$, f_{23}^{π} omitted

HJET at RHIC operated in safe region around $B_y = 120\,\mathrm{mT}$

- At RHIC, transitions with $\frac{f_{ij}}{f_b^{\mathrm{RHIC}}} \gtrsim 350$ were ignored
- Don't know exactly at which harmonic number, depolarization sets in.

Single bunch distribution

- (Gaussian) bunch in EIC

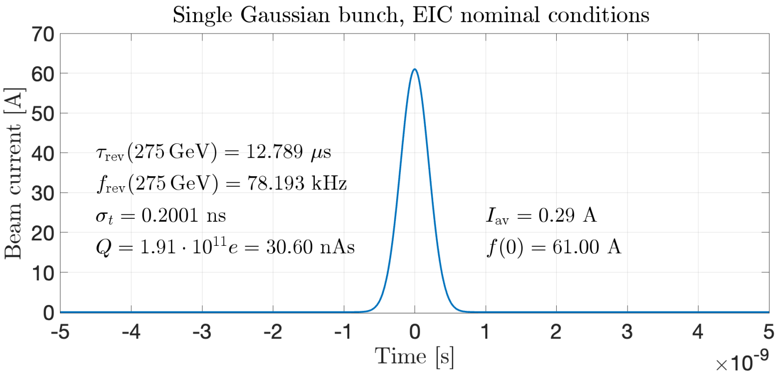

Pulse shape described by

$$f(t) = \frac{Q}{\sqrt{2\pi}\sigma_t} \exp\left(-\frac{t^2}{2\sigma_t^2}\right) \quad (11)$$

Bunch structure

EIC situation:

- Time period between two adjacent bunches: $\tau_\mathrm{b} = \frac{\tau_\mathrm{rev}}{N_b} = 10.85\,\mathrm{ns}$
- Number of stored bunches $N_b = 1160$
- Bunch frequency $f_\mathrm{b} = \frac{1}{\tau_\mathrm{b}} = 92.2081\,\mathrm{MHz}$

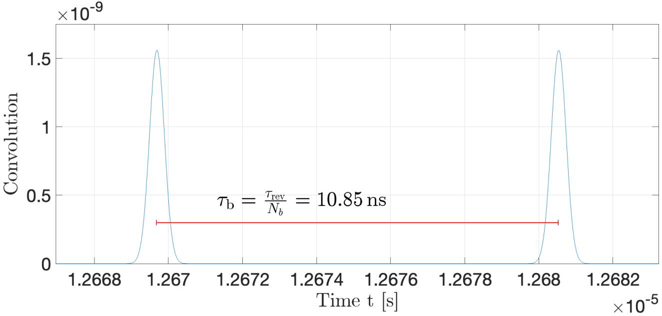

Gaussian convoluted with (finite) series of delta functions

Total beam current as function of time t given by

$$I(t) = \int_{-\infty}^{\infty} f(t-\xi) \sum_{k=-\infty}^{\infty} \delta\left(\xi - k\frac{\tau_{\mathrm{rev}}}{N_{\mathrm{b}}}\right) \mathrm{d}\xi \qquad (12)$$

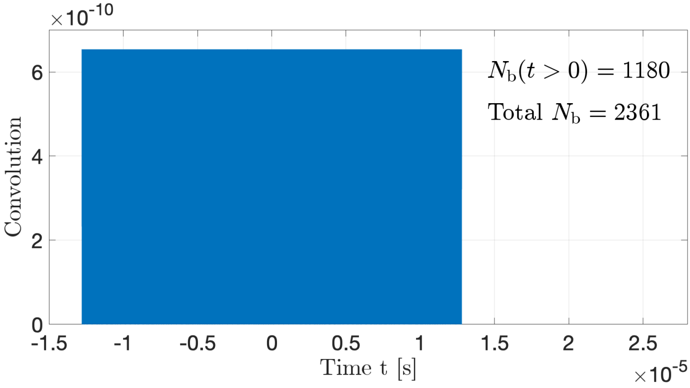

Produced radio-frequency fields

- Single-sided amplitude spectrum of FFT

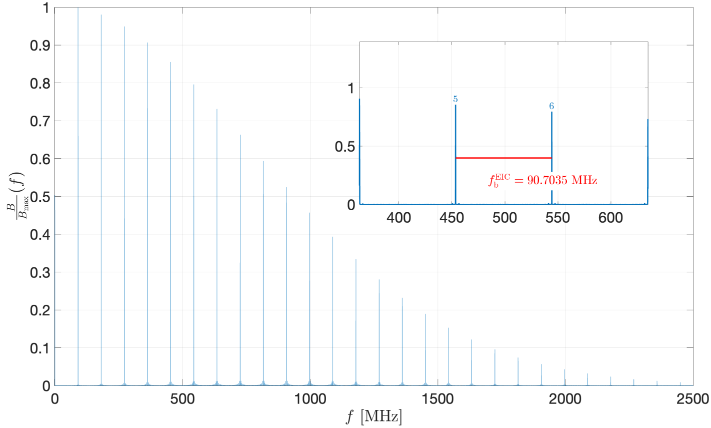

Amplitudes of radio-frequency fields

- Frequency spacing becomes larger at EIC ⇒ fewer resonances contribute
- RF field amplitudes at EIC ≈ 10× larger compared to RHIC
  ⇒ increased transition probability due more photons ($n_\gamma \propto B^2$).

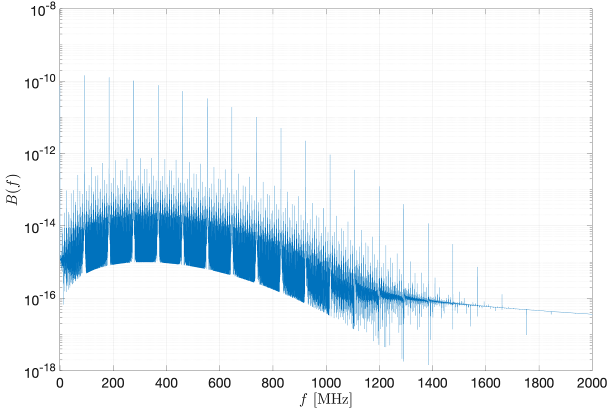

Hyperfine transitions in H from bunch fields at EIC

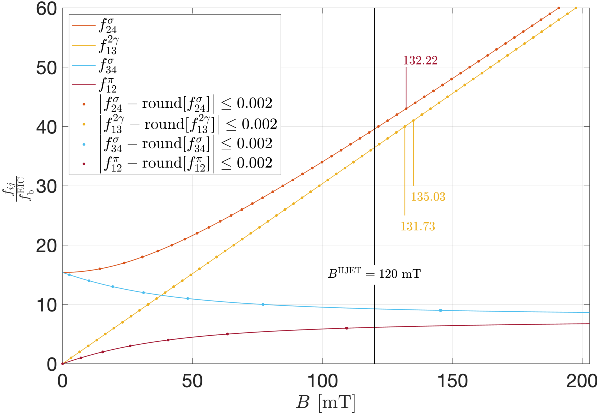

Depolarization (numerically) occurs when

$$\left|\frac{f_{ij}}{f_b^{\mathrm{EIC}}} - n\right| \leq 0.002\,,\ n \in \mathbb{N}$$

In contrast to RHIC, for $B < 200\,\mathrm{mT}$

- **all transitions below harmonic number** ≈ 60 **contribute at EIC!**

Hyperfine transitions in H from bunch fields at EIC

How about the region of small B?

- At RHIC, this region was inaccessible, as spacing of $f_{13}^{2\gamma} \approx 0.3\,\text{mT}$.
- At EIC, at $\approx 5\,\text{mT}$, spacing of $f_{13}^{2\gamma} \approx 3.3\,\text{mT}$.

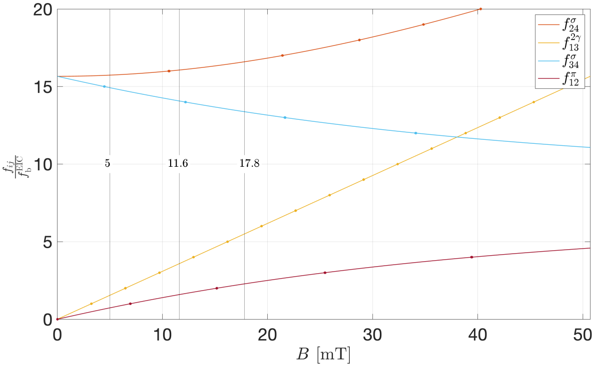

Magnetic field from beam charge

RHIC

Moving charge of beam induces magnetic field at HJET target

- β functions at the HJET in IP12 from G. Robert-Demolaize, 23.07.2024 for RHIC at top energy, determined from fill #34819,

$$\begin{aligned} \beta_x &= 8.243\,\mathrm{m}, \beta_y = 8.326\,\mathrm{m} \\ \beta_x &= 8.303\,\mathrm{m}, \beta_y = 8.252\,\mathrm{m} \end{aligned} \tag{13}$$

- Assume in the following an average $\bar{\beta}_{\text{jet}} = 8.281$
- Since $\beta_x \approx \beta_y$, we deal with a round beam. The normalized RMS emittance taken from the RHIC dashboard during run 24 is:

$$\varepsilon^N_{\text{rms}} = 2.5\,\mu\mathrm{m}\,. \tag{14}$$

Beam parameters for RHIC

- For a Gaussian beam, assume a current density of

$$J = \frac{I(t)}{2\pi\sigma_r^2} \exp\left(-\frac{r^2}{2\sigma_r^2}\right) , \quad \text{where} \quad \sigma_r = \sqrt{\frac{\bar{\beta}_{\text{jet}}\epsilon^{\text{N}}_{\text{rms}}}{k\cdot\beta\gamma}} \tag{15}$$

- Due to symmetry of problem, magnetic field $\vec{B}$ will be tangential to concentric circles around z-axis. Thus, $\vec{B}$ can be written as

$$\vec{B} = B(r)\vec{e}_\phi \tag{16}$$

- With beam traveling in $\vec{e}_z$ direction, the integration for a cylindrical Gaussian beam yields flux density

$$\boxed{\vec{B}(r) = \frac{\mu_0 I(t)}{2\pi r}\left[1-\exp\left(-\frac{r^2}{2\sigma_r^2}\right)\right]\vec{e}_\phi\text{ , with }\vec{e}_\phi = \vec{e}_z\times\vec{e}_r} \tag{17}$$

-

Emittance[1]	Beam width	injection 23.5 GeV	flattop 250 GeV
$\epsilon^N_{\text{rms}} = 2.5\,\mu\text{m}$	$\sigma_r^{1\sigma} = \left(\bar{\beta}_{\text{jet}}\cdot\frac{\epsilon^N_{\text{rms}}}{\beta\gamma}\right)^{\frac{1}{2}}$	0.89 mm	0.28 mm
$\epsilon^N_{95} = \epsilon^N_{\text{rms}}\cdot 5.993$	$\sigma_r^{95} = \sigma_r^{1\sigma}\cdot\sqrt{5.993}$	2.18 mm	0.68 mm

[1] Factor 5.993 to convert 1D rms emittance to emittance for 95% of particles in a beam [5].

Magnetic field from beam charge at RHIC

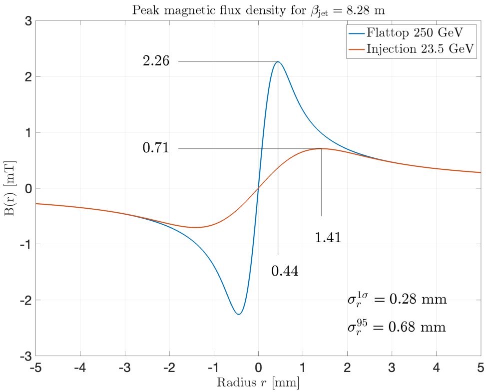

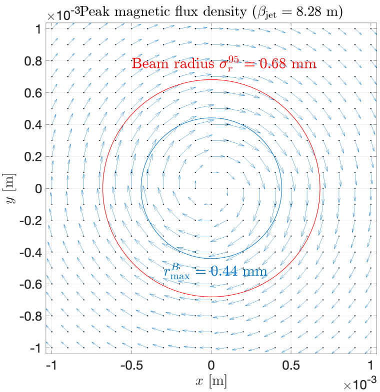

Situation when peak of bunch hits target

Effect of induced magnetic field on jet pol at RHIC

- Systematic variation of magnetic holding field in region struck by beam:
- In center ($r = 0$), $|\vec{B}(r)| = B_y^{\text{nom}} = 120\,\text{mT}$
- Inside beam, magnetic fields are modified

$$\frac{\int_0^{\sigma_r^{95}} B(r)\text{d}r}{\sigma_r^{95}} = 1.73\,\text{mT} \tag{18}$$

- In midplane ($y = 0$), still $\vec{B} \parallel \vec{e}_y$.
  - Left hemishere: $\bar{B}^{\text{L}} = 121.73\,\text{mT}$, Right hemishere: $\bar{B}^{\text{R}} = 118.27\,\text{mT}$

  Relative change of target polarization inside beam is, e.g.,

$$\delta P = \frac{P_{|1\rangle+|4\rangle}(\bar{B}^{\text{L}}) - P_{|1\rangle+|4\rangle}(\bar{B}^{\text{R}})}{P_{|1\rangle+|4\rangle}(B_y^{\text{nom}})} \leq 0.21\% \tag{19}$$

- In vertical plane ($x = 0$), $\vec{B} \nparallel \vec{e}_y$.

Conclusion for RHIC

- No depolarization due to variation of B inside beam (slide 18)
- Effect small/tolerable in terms of syst. contribution to jet polarization

Beam parameters

EIC

EIC beam parameters taken from Conceptual Design Report [6]

- 275 GeV
- β-functions:
    - $\beta_x = 230.323\,\text{m}$
    - $\beta_y = 69.935\,\text{m}$
    - $\rightarrow$ assumed in the following: $\bar{\beta} \approx 150\,\text{m}$ for future location of HJET at IP4 (from H. Lovelace, 31.07.2024).
- Like before, $\epsilon_{95}^{N} = \epsilon_{\text{rms}}^{N} \cdot 5.993$
- Two situations for IP4:

Beam	$\epsilon_{\text{rms}}^{N}$ [µm]	$\sigma_r^{1\sigma}$ [mm]	σ_r^{95} [mm]
uncooled	2.5	1.13	2.76
cooled	0.47	0.49	1.20

Magnetic field from beam charge

EIC

Uncooled beam

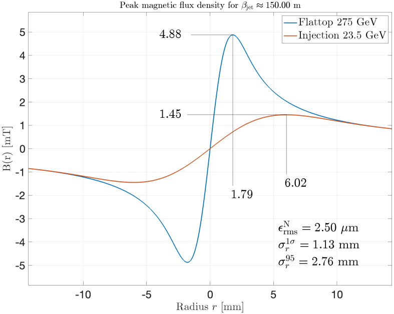

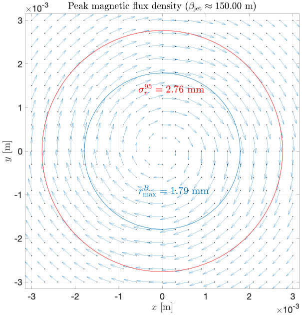

HJET beam size

- On flattop, transverse dimensions of uncooled proton beam at IP4 comparable to HJET beam diameter (6 mm FWHM $\rightarrow \sigma^{\text{HJET}} \approx 2.55$ mm).

Magnetic field from beam charge

EIC

Cooled beam

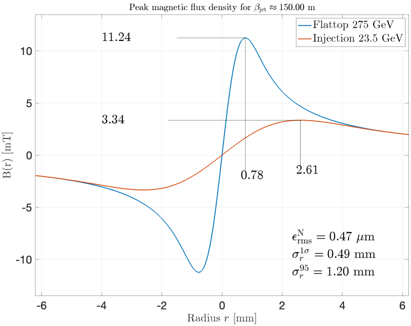

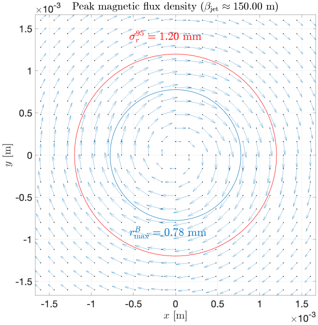

Effect on magnetic field at jet target and its polarization

EIC

Implications for EIC

1. Induced B field from beam charge:
   - uncooled beam: $B(r) \leq 4.88\,\mathrm{mT}$
   - cooled beam: $B(r) \leq 11.74\,\mathrm{mT}$

   $\rightarrow$ kills idea to apply weak holding field (20 mT) at target (slide 25)
2. Variation of polarization inside target area at 120 mT [Eq. (19)]:
   - uncooled beam: $\delta P = 0.45\%$
   - cooled beam: $\delta P = 1.05\%$
3. Variation of polarization inside target area at 300 mT [Eq. (19)]:
   - uncooled beam: $\delta P = 0.1\%$
   - cooled beam: $\delta P = 0.1\%$
4. **Due to fields induced by beam charge (item 1), beam-induced depolarizing resonances appear in HJET target** (slide 24)

Mitigation of beam-induced magnetic field effect at EIC

Possible solutions

1. At RHIC, B-field was moved to $\approx 120\,\mathrm{mT}$ and $\frac{f_{ij}}{f_\mathrm{b}^\mathrm{RHIC}} \geq 350$ ignored (slide 18)
2. **Strategy for EIC:** $\Rightarrow$ **push harmonics to** $\geq 100 \Rightarrow$ **holding field** $\geq 350\,\mathrm{mT}$

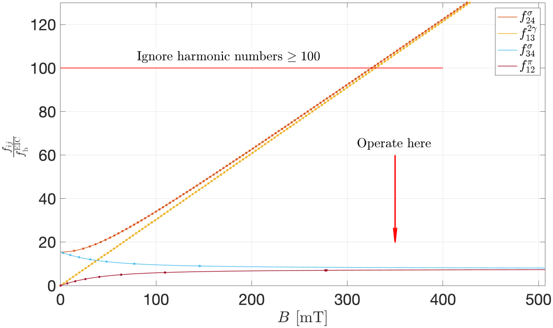

Where exactly is cutoff located for f^σ_{24} and $f^{2\gamma}_{13}$?

- What is known from RHIC or could still be learned about at which B field, harmonics become harmless?

Concept for magnetic guide field for HJET at EIC

But first ...

Spin-dependent *pp* elastic cross section (spin 1/2 + spin 1/2)

With polarized beam $\vec{P}$ and polarized target $\vec{Q}$, all components of $\vec{P}$ can be determined from spin-dependent cross section, as shown in Refs. [7, 8]:

$$
\begin{aligned}
\sigma/\sigma_0 = 1 + A_y & \left[(P_y + Q_y)\cos\phi - (P_x + Q_x)\sin\phi\right] \\
& + A_{xx}\left[P_x Q_x \cos^2\phi + P_y Q_y \sin^2\phi + (P_x Q_y + P_y Q_x)\sin\phi\cos\phi\right] \\
& + A_{yy}\left[P_x Q_x \sin^2\phi + P_y Q_y \cos^2\phi - (P_x Q_y + P_y Q_x)\sin\phi\cos\phi\right] \\
& + A_{xz}\left[(P_x Q_z + P_z Q_x)\cos\phi + (P_y Q_z + P_z Q_y)\sin\phi\right] + A_{zz} P_z Q_z
\end{aligned}
$$

- Full angular distributions of all A_{ik}'s were determined.
- Single input: $A_y = 0.2122 \pm 0.0017$ at $\theta_{\text{lab}} = 8.64^\circ \pm 0.07^\circ$ [9], known from $A_y = 1$ point in $p + {}^{12}\text{C}$ elastic scattering [10].

Most importantly in context

- determination of beam $\vec{P} = (P_x, P_y, P_z)$ and target $\vec{Q} = (Q_x, Q_y, Q_z)$, as well as non-flipping components possible (slide 36)

Polarization of beam $\vec{P}$ and target $\vec{Q}$ [7, 8]

	$\pm x$		$\pm y$		$\pm z$	
	PRE	POST	PRE	POST	PRE	POST
P_x	0.0052(47)	0.0089(44)	0.0052(47)	0.0089(44)	0.0052(47)	0.0089(44)
P_y [a]	**0.5801(34)**	**0.5425(32)**	**0.5802(34)**	**0.5417(32)**	**0.5765(34)**	**0.5447(32)**
P_z	−0.0021(47)	0.0003(44)	−0.0021(47)	0.0003(44)	−0.0021(47)	0.0003(44)
Q_x	**0.7401(59)**	**0.7394(56)**	−0.0039(59)	0.0039(56)	−0.0071(23)	−0.0052(23)
Q_y	0.0111(59)	0.0039(56)	**0.7400(59)**	**0.7406(56)**	−0.0055(59)	−0.0034(56)
Q_z	0.0158(60)	0.0240(60)	−0.0174(61)	−0.0121(61)	**0.7401(42)** [b]	**0.7400(40)** [b]
S_{P_y}	−0.0008(18)	−0.0005(17)	−0.0008(18)	0.0005(17)	−0.0008(18)	0.0005(17)
S_{Q_x}	0.0017(23)	−0.0007(23)	−0.0040(23)	−0.0031(23)	−0.0043(23)	−0.0024(23)
S_{Q_z}	−0.0091(82)	−0.0162(82)	−0.0177(82)	−0.0197(82)	0.0013(82)	−0.0086(82)

- With two flattops, beam polarization export/calibration arbitrary energy [11]

- PRE $\equiv$ b (197.4 MeV)
- Export $\equiv$ c (399.1 MeV)
- POST $\equiv$ d (197.4 MeV)

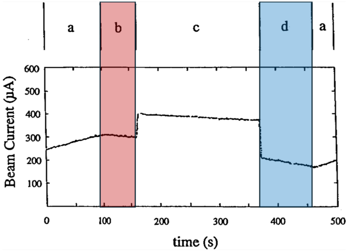

Spin-dependent *pp* elastic cross section

The above is relevant for two reasons

1. The spin-dependence of $\vec{p}\vec{p}$ elastic scattering allows to reconstruct angular distributions of all (in that case five) polarization observables.
2. With suitable magnetic guide field, target polarization $\vec{Q}$ can be oriented along any direction, for instance along x, so that $\vec{Q} = Q \cdot \vec{e}_x = \vec{Q}_x$
   - Absolute value of target polarization Q determined by BRP

Two things needed to port HJET from RHIC to EIC with $\frac{\Delta P}{P} \leq 1\%$

1. Substantially stronger holding field of $|\vec{B}| \approx 300$ to $350\,\mathrm{mT}$ than at RHIC
2. Detector capable to pick up azimuthal asymmetries $\propto \sin\phi$ and $\propto \sin 2\phi$ (slide 38)
   - foresee detector symmetry to provide $\vec{d}\vec{d}$ beam absolute polarimetry, i.e., beyond $\propto \sin 2\phi$.

Detector symmetry required to accomplish the task

For spin $\frac{1}{2}$ + spin $\frac{1}{2}$ scattering, suitable geometry below shows pattern of detected azimuthal angles [7].

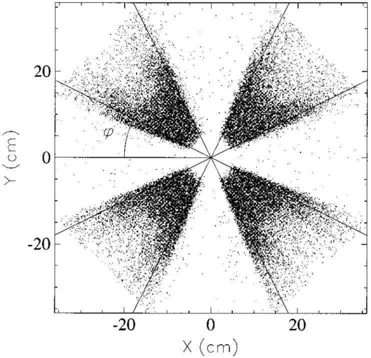

For spin $\frac{1}{2}$ + spin 1 scattering, a higher segmentation is needed, because besides $\sin\phi$ and $\sin 2\phi$, also terms $\sin 3\phi, \ldots$ contribute to asymmetries [12].

Holding field system for $|\vec{B}| \approx 0.3\,\mathrm{T}$ with $\vec{B} \parallel \vec{e}_{x,y,z}$

Work in part together with Helmut Soltner (FZJ, Germany)

Motivation:

- Reconcile strong magnetic holding field with open detector geometry to determine, e.g., all spin components of beam polarization $\vec{P} = (P_x, P_y, P_z)$
- Exploit magnetic moments $\vec{m}$ of homogeneously magnetized spheres [13–15]
- Invert $\vec{m}$ in vacuum to reverse $\vec{B}(O)$
- Reorient $\vec{m}$'s to generate $\vec{B}(O) \parallel \vec{e}_{x,y,z}$

Consider two sets of frames

- Beam meets atoms at (O)
  - Set 1: $100\,\mathrm{mm}_x \times 100\,\mathrm{mm}_y \times 40\,\mathrm{mm}_z$
  - Set 2: $100\,\mathrm{mm}_x \times 100\,\mathrm{mm}_y \times 110\,\mathrm{mm}_z$
  - 8 magnetized spheres in corners of frames:
  - NeFeB magnets provide remanence of $B_r = 1.49 - 1.55\,\mathrm{T}$ (type N58)
  - Radius $r = 30\,\mathrm{mm}$

Holding field system: Calculation

- Flux density vector as fct of $\vec{m}$ in space

$$\vec{B}(\vec{r}) = \frac{\mu_0}{4\pi}\left[\frac{3\left(\vec{m}\cdot\hat{R}\right)\hat{R}-\vec{m}}{|R|^3}\right] \quad (20)$$

$$\vec{R} = \vec{r} - \vec{r}_0, \hat{R} = \frac{\vec{R}}{|R|}$$

- Optimize orientation of $\vec{m}$'s to maximize $\vec{B}(O)$ along $\vec{e}_x$, $\vec{e}_y$, or $\vec{e}_z$
  - maximize dot product $\vec{m}\cdot\hat{R}$, set $m_y = 0$ to obtain, e.g., max. B_y

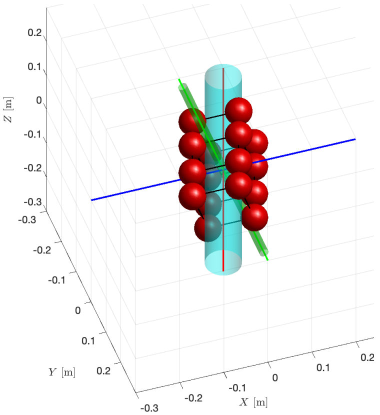

16 spherical magnetic dipoles

- atomic beam $\parallel \vec{e}_y$
- ion beam $\parallel \vec{e}_z$

Component $B_x(O)$ using two sets of $\vec{m}$'s

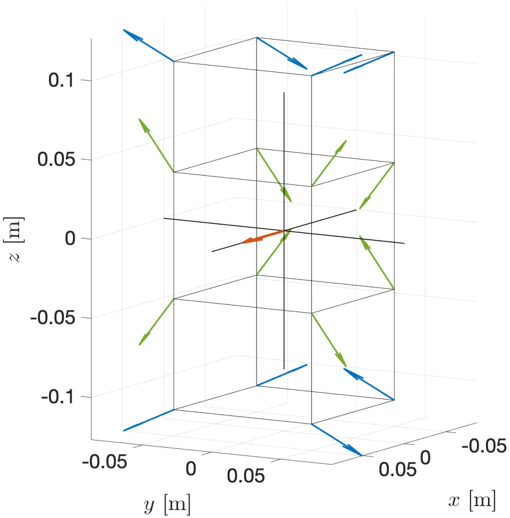

$$B_x: \begin{pmatrix} 0.3224 \\ 0 \\ 0 \end{pmatrix} \text{T}$$

Component $B_y(O)$ using two sets of $\vec{m}$'s

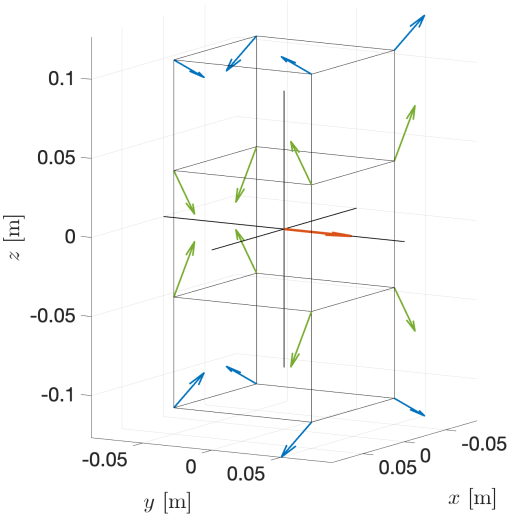

$$B_y: \begin{pmatrix} 0 \\ 0.3224 \\ 0 \end{pmatrix} \mathrm{T},$$

Component $B_z(O)$ using two sets of $\vec{m}$'s

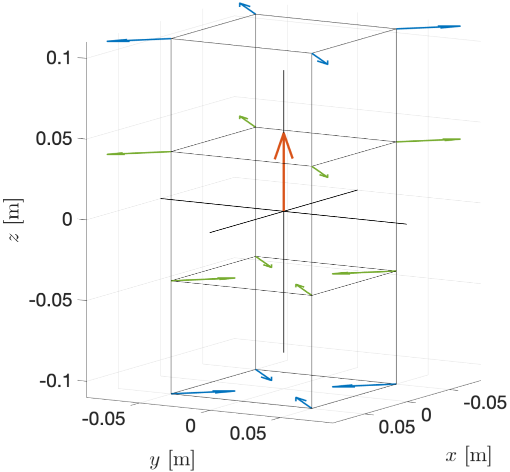

$$B_z: \begin{pmatrix} 0 \\ 0 \\ 0.3227 \end{pmatrix} \text{T}$$

Technical realization

LDRD C application (approved)

With properly rotated spheres

- Setup allows for azimuthally symmetric detector setup with acceptance $\Delta\phi \approx \pm 20^\circ$ at $\phi = 45$, 135, 225, and 315°
  - Slide 38 shows how azimuthal acceptance could look like
- **Technical challenges:**
  1. Accurate 3D reorientation of magnetized spheres in vacuum [16]
  2. Vacuum compatible coating of magnets, e.g., Ni, or stainless steel covers to prevent H and H_2 from deteriorating NeFeB
  3. **First Step: build a lab test setup and verify concept is technically sound**
  4. Forces and torques appear manageable (next slides)

Active ball joint mechanism with spherical gears [16]

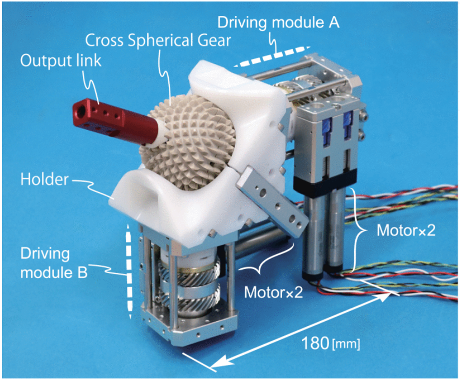

https://www.youtube.com/watch?v=hhDdfiRCQS4

Force and torque between two dipoles $\vec{m}_1$ and $\vec{m}_2$ I

Potential energy of magnetic dipole

$$U = -\vec{m} \cdot \vec{B}$$
$$\vec{F} = -\vec{\nabla} U \quad \rightarrow \quad F_{12} = \vec{\nabla}\left(\vec{m}_2 \cdot \vec{B}_1\right) \tag{21}$$

- $\vec{B}_1$ is flux density produced by $\vec{m}_1$ at location of $\vec{m}_2$.

Force

$$\vec{F}_{12}(\vec{r}_{12}, \vec{m}_1, \vec{m}_2) = \frac{3\mu_0}{4\pi r_{12}^4}\Big[\vec{m}_2\left(\vec{m}_1 \cdot \vec{e}_{12}\right) + \vec{m}_1\left(\vec{m}_2 \cdot \vec{e}_{12}\right) + \vec{e}_{12}\left(\vec{m}_1 \cdot \vec{m}_2\right) - 5\vec{e}_{12}\left(\vec{m}_1 \cdot \vec{e}_{12}\right)\left(\vec{m}_2 \cdot \vec{e}_{12}\right)\Big] \tag{22}$$

- $\vec{r}_{12}$ is vector between $\vec{m}_1$ and $\vec{m}_2$, $\vec{e}_{12} = \frac{\vec{r}_{12}}{|r_{12}|}$.

Torque

$$\vec{\tau} = \vec{m}_2 \times \vec{B}_1 \tag{23}$$

Force and torque between two dipoles $\vec{m}_1$ and $\vec{m}_2$ II

Examples: $\vec{m}_1 \perp \vec{m}_2$

1. **Spheres touch:**

$$r_{12} = 0.06\,\mathrm{m} \quad \vec{F}_{12} = -417\,\mathrm{N} \quad \tau_{12} = 8.3\,\mathrm{Nm} \tag{24}$$

2. **System assembled** (slide 40):

$$r_{12} \geq 0.07\,\mathrm{m} \quad \vec{F}_{12} \leq -225\,\mathrm{N} \quad \tau_{12} = 5.2\,\mathrm{Nm} \tag{25}$$

Flux density of system in 3D

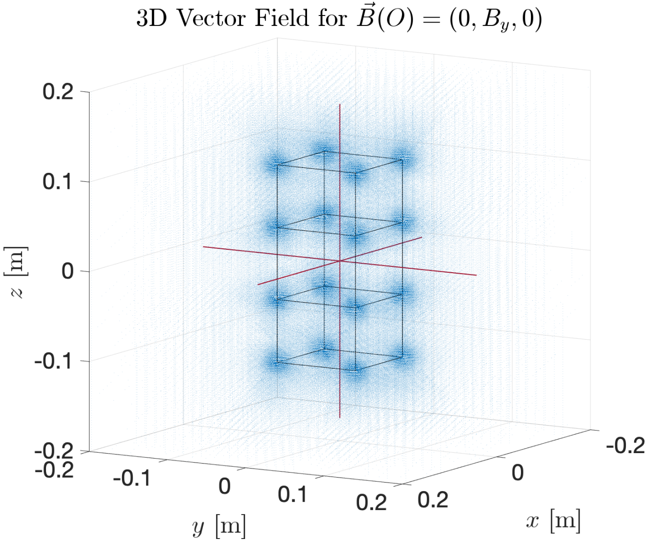

No zero crossings along axes

$\vec{B}(O) \parallel \vec{e}_x$

$\vec{B}(O) \parallel \vec{e}_y$

$\vec{B}(O) \parallel \vec{e}_z$

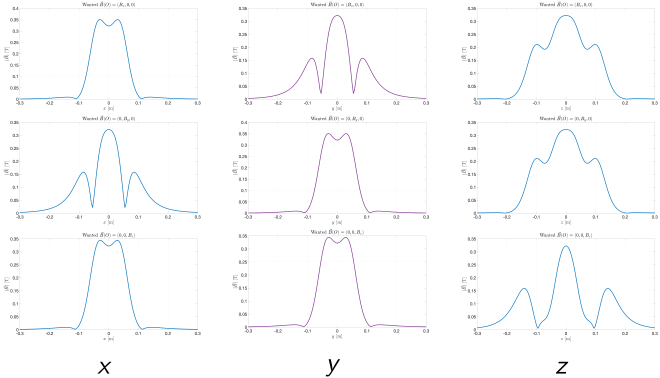

- No zero crossing of magnetic field along vertical jet (y) axis
- $B_y^{\min} \approx 1.9\,\mathrm{mT}$ sufficient to avoid Majorana depolarization
- Field integrals along beam (z) axis

$\vec{B}(O)$	$\parallel \vec{e}_x$	$\parallel \vec{e}_y$	$\parallel \vec{e}_z$
$\int \lvert\vec{B}\rvert \mathrm{d}z$	$0.0667\,\mathrm{Tm}$	$0.0667\,\mathrm{Tm}$	$0.0546\,\mathrm{Tm}$

Polarized ^{3}He Atomic Beam Source

Original MIT development for nEDM experiment at Oakridge ORNL

- Prajwal T. MohanMurthy, J. Kelsey, J. Dodge, R. Redwine, R. Milner, P. Binns, B. O'Rourke
- nEDM experiment at ORNL discontinued

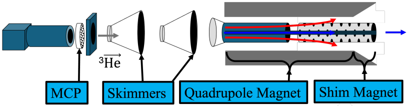

$^3\vec{\mathrm{He}}$: quadrupole magnet selects spins
- **1.3 K ≈ 86 μeV**
- $\Delta E = \mu_m \approx 67$ neV/T
- initial angle very important

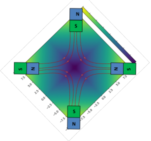

High atomic flux

- $\geq 1 \times 10^{14}$ atoms/s $\quad \rightarrow \quad d_t \geq 1 \times 10^{13}$ atoms/cm^2
- Ideal device for absolute $^3\vec{\mathrm{He}}^{++}$ beam polarimetry at EIC

Absolute polarimetry of $\vec{d}$ beams

Polarized atomic deuterium jet

- Atomic beam sources like the HJET efficiently produce also beams of deuterium atoms
- Ideal would be the use of dual-function RF transition units for $\vec{\mathrm{H}}$ and $\vec{\mathrm{D}}$ atoms, as these wouldn't require to break vacuum
- With vector and tensor polarization accurately determined by BRP, absolute beam polarimetry based on $\vec{d}\vec{d}$ elastic scattering becomes possible
  - $+$ reconstruction of 3D polarization vector, including tensor components.

Example: H and D polarizations from the ANKE ABS [17]

Beam	Populated state(s)	p_z	p_{zz}
Hydrogen	$\|1\rangle$	$+0.89 \pm 0.01$	–
	$\|3\rangle$	-0.96 ± 0.01	–
Deuterium	$\|1\rangle + \|6\rangle$	$+0.88 \pm 0.01$	$+0.88 \pm 0.03$
	$\|3\rangle + \|4\rangle$	-0.91 ± 0.01	$+0.85 \pm 0.02$
	$\|3\rangle + \|6\rangle$	$+0.005 \pm 0.003$	$+0.90 \pm 0.01$
	$\|2\rangle + \|5\rangle$	$+0.005 \pm 0.003$	-1.71 ± 0.03

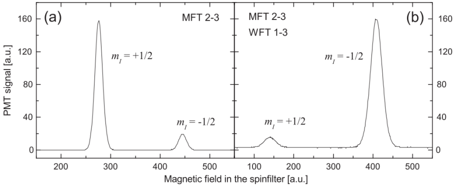

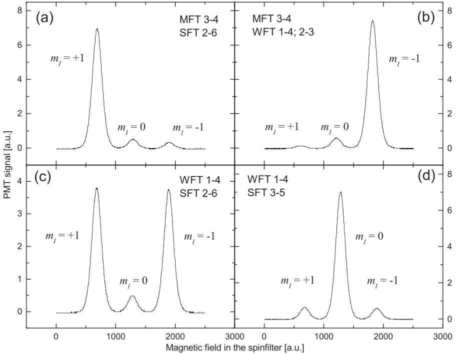

EIC hadron polarimetry at IP4

Carbon, polarized H and ^{3}He gas targets

- Important to set up all polarimeters in one place without much drift, magnetic elements, etc, to minimize spin rotation between them

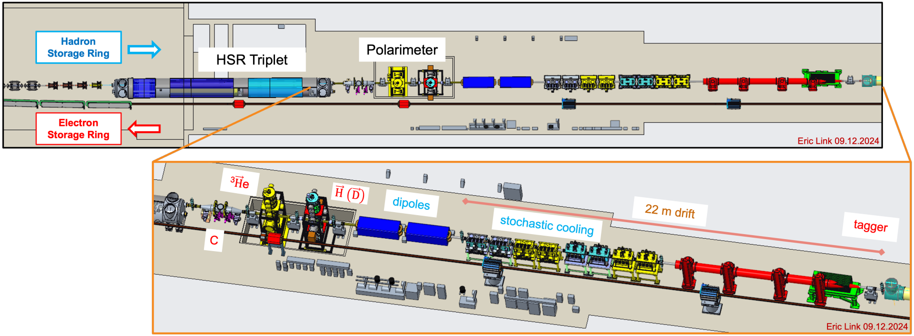

Conclusion and Outlook I

1. **Bunch-induced depolarization in H target**
   - RHIC: harmonic numbers > 350 were ignored
   - EIC: All depolarizing transitions appear at harmonic numbers < 50
2. **Beam-induced magnetic fields perturb target polarization**
   - RHIC: Magnetic field involved: $B(r) \leq 2.3\,\mathrm{mT}$
   - EIC: uncooled $B(r) < 4.9\,\mathrm{mT}$
   - EIC: cooled $B(r) < 11.7\,\mathrm{mT}$
3. **Solution for 1. and 2.: Holding field of $|\vec{B}| \geq 300\,\mathrm{mT}$**
   - Concept using permanent magnets (NdFeB) appears feasible
     - **FY2025 LDRD C approved to build a demonstrator**
   - Allows for orientation of holding field $\vec{B}$ in any direction (along x, y, or z)
   - System will allow to provide holding field $\vec{B} = 0$
   - No zero crossings along ABS axis, $|\vec{B}(0, y, 0)| \gtrsim 1.9\,\mathrm{mT}$
   - May need compensation scheme to make $\int B_{x,y,z} \mathrm{d}\ell = 0$ along beam (z) axis
     - What's the spin rotation angle along the beam (z) axis? Tolerable?
     - Does one need compensation beyond $\int B \mathrm{d}\ell = 0$?

Conclusion and Outlook II

4. **Early 2026: HJET set up in high bay of 510**
    - Refurbish and upgrade system
    - Upgrade slow control
    - Implement QMA in setup to determine H_1 and H_2 contribution in the target
5. **$^3\vec{\mathrm{He}}$ atomic beam source under development by MIT**
    - ideally suited for EIC
    - Polarimetry section in IP4 looks good
6. **$\vec{\mathrm{D}}$ and $^3\vec{\mathrm{He}}$ atomic targets at EIC**
    - Study bunch-induced depolarization
    - Study beam-induced $\vec{B}$ field effects on target polarizations

Conclusion and Outlook III

Other things that need to be looked into

1. Zero-crossings along the vertical axis of present HJET
   - Revisit magnetic field calculations of HJET holding field → in progress.
   - Measure holding field in target region and estimate present hysteresis effects
2. Carry out a polarization measurements at HJET using all RF transition units in ABS and BRP after run 25.
3. **Top Priority:** Regain ability to simulate/design polarized atomic beams
   - Critical competence, disappeared from academia in both the US and Europe, **foundational step, absolutely essential**, underpins all future progress.
   - Tracking code used originally for HJET design recuperated from Michelle Stancari/Paolo Lenisa → will be time consuming to make it work
   - A **postdoc of 2 years** will be sufficient to revitalize the critical atomic beam tracking instruments and restore the necessary simulation capabilities
     - **FY2025 LDRD B application pending:** Zhengqiao Zhang (BNL) started to look into this

Back to my initial observation

- Key issues include funding, talent recruitment, and securing long-term commitment of new partner institutions
- Future of spin physics with $\vec{d}$, $^{3}\overrightarrow{\mathrm{He}}^{++}$, or $^{6,7}\overrightarrow{\mathrm{Li}}$ beams will no longer even be an option if we wait a few more years to get our act together
- Organize workshops and attract groups from national and international scientific community to work on polarization technology
- **Next step:**

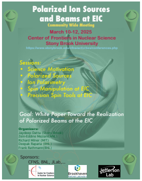

$\Rightarrow$ **Produce a White Paper**

References I

[1] W. Haeberli, “H-jet measures beam polarization at RHIC,” CERN Cour. **45N8**, 15 (2005).

[2] M. Diermaier, C. B. Jepsen, B. Kolbinger, C. Malbrunot, O. Massiczek, C. Sauerzopf, M. C. Simon, J. Zmeskal, and E. Widmann, “In-beam measurement of the hydrogen hyperfine splitting and prospects for antihydrogen spectroscopy,” Nature Commun. **8**, 5749 (2017), 1610.06392.

[3] A. Airapetian, N. Akopov, Z. Akopov, M. Amarian, A. Andrus, E. Aschenauer, W. Augustyniak, R. Avakian, A. Avetissian, E. Avetissian, et al., “The hermes polarized hydrogen and deuterium gas target in the hera electron storage ring,” Nuclear Instruments and Methods in Physics Research Section A: Accelerators, Spectrometers, Detectors and Associated Equipment **540**, 68 (2005), ISSN 0168-9002, URL https://www.sciencedirect.com/science/article/pii/S0168900204024167.

[4] N. Ramsey, *Molecular Beams* (Oxford University Press, 1956).

[5] S. Lee, *Accelerator Physics* (World Scientific Publishing Company, 2011), ISBN 9789814405287.

[6] F. Willeke and J. Beebe-Wang, “Electron ion collider conceptual design report 2021,” (????), URL https://www.osti.gov/biblio/1765663.

[7] F. Rathmann et al., “Complete angular distribution measurements of pp spin correlation parameters Axx, Ayy, and Axz and analyzing power Ay at 197.4 MeV,” Phys. Rev. C **58**, 658 (1998).

[8] B. von Przewoski et al., “Proton proton analyzing power and spin correlation measurements between 250-MeV and 450-MeV at $7^\circ \leq \theta(c.m.) \leq 90^\circ$ with an internal target in a storage ring,” Phys. Rev. C **58**, 1897 (1998).

[9] B. von Przewoski, H. O. Meyer, P. V. Pancella, S. F. Pate, R. E. Pollock, T. Rinckel, F. Sperisen, J. Sowinski, W. Haeberli, W. K. Pitts, et al., “Absolute measurement of the p+p analyzing power at 183 mev,” Phys. Rev. C **44**, 44 (1991), URL https://link.aps.org/doi/10.1103/PhysRevC.44.44.

[10] G. Plattner and A. Bacher, “Absolute calibration of spin-$\frac{1}{2}$ polarization,” Physics Letters B **36**, 211 (1971), ISSN 0370-2693, URL https://www.sciencedirect.com/science/article/pii/0370269371900712.

References II

[11] R. E. Pollock, W. A. Dezarn, M. Dzemidzic, J. Doskow, J. G. Hardie, H. O. Meyer, B. v. Przewoski, T. Rinckel, F. Sperisen, W. Haeberli, et al., "Calibration of the polarization of a beam of arbitrary energy in a storage ring," Phys. Rev. E **55**, 7606 (1997), URL `https://link.aps.org/doi/10.1103/PhysRevE.55.7606`.

[12] B. v. Przewoski et al., "Analyzing powers and spin correlation coefficients for $p + d$ elastic scattering at 135 and 200 MeV," Phys. Rev. C **74**, 064003 (2006), URL `http://link.aps.org/doi/10.1103/PhysRevC.74.064003`.

[13] P. Blümler and H. Soltner, "Practical Concepts for Design, Construction and Application of Halbach Magnets in Magnetic Resonance," Applied Magnetic Resonance **54**, 1701 (2023), ISSN 1613-7507, URL `https://doi.org/10.1007/s00723-023-01602-2`.

[14] H. Soltner and P. Blümler, "Dipolar halbach magnet stacks made from identically shaped permanent magnets for magnetic resonance," Concepts in Magnetic Resonance Part A **36A**, 211 (2010), `https://onlinelibrary.wiley.com/doi/pdf/10.1002/cmr.a.20165`, URL `https://onlinelibrary.wiley.com/doi/abs/10.1002/cmr.a.20165`.

[15] H. Raich and P. Blümler, "Design and construction of a dipolar halbach array with a homogeneous field from identical bar magnets: Nmr mandhalas," Concepts in Magnetic Resonance Part B: Magnetic Resonance Engineering **23B**, 16 (2004), `https://onlinelibrary.wiley.com/doi/pdf/10.1002/cmr.b.20018`, URL `https://onlinelibrary.wiley.com/doi/abs/10.1002/cmr.b.20018`.

[16] K. Abe, K. Tadakuma, and R. Tadakuma, "Abenics: Active ball joint mechanism with three-dof based on spherical gear meshings," IEEE Transactions on Robotics **37**, 1806 (2021).

References III

[17] M. Mikirtychyants, R. Engels, K. Grigoryev, H. Kleines, P. Kravtsov, S. Lorenz, M. Nekipelov, V. Nelyubin, F. Rathmann, J. Sarkadi, et al., "The polarized h and d atomic beam source for {ANKE} at cosy-jülich," Nuclear Instruments and Methods in Physics Research Section A: Accelerators, Spectrometers, Detectors and Associated Equipment **721**, 83 (2013), ISSN 0168-9002, URL `http://www.sciencedirect.com/science/article/pii/S0168900213003483`.

[18] N. Akchurin, J. Langland, Y. Onel, B. E. Bonner, M. D. Corcoran, J. Cranshaw, F. Nessi-Tedaldi, M. Nessi, C. Nguyen, J. B. Roberts, et al., "Analyzing power measurement of pp elastic scattering in the coulomb-nuclear interference region with the 200-gev/c polarized-proton beam at fermilab," Phys. Rev. D **48**, 3026 (1993), URL `https://link.aps.org/doi/10.1103/PhysRevD.48.3026`.

[19] I. G. Alekseev, A. Bravar, G. Bunce, S. Dhawan, K. O. Eyser, R. Gill, W. Haeberli, H. Huang, O. Jinnouchi, A. Kponou, et al., "Measurements of single and double spin asymmetry in *pp* elastic scattering in the cni region with a polarized atomic hydrogen gas jet target," Phys. Rev. D **79**, 094014 (2009), URL `https://link.aps.org/doi/10.1103/PhysRevD.79.094014`.

[20] N. H. Buttimore, "A Helium-3 polarimeter using electromagnetic interference," PoS **PSTP2013**, 057 (2013).

[21] M. Planck, *The Theory of Heat Radiation* (P. Blakiston's Son & Co., 1914).

Spare slides

Coulomb-Nuclear interference I

Need for calibration

- Asymmetry from CNI region constitutes basis of RHIC high-energy (absolute) polarimeters
  - derived from same EM amplitude that generates anomalous magnetic moment

$$\mu_p = g_p \frac{e\hbar}{2m_p} = g_p \mu_N, \quad g_p \approx 5.585$$
$$g_p - 2 \approx 3.585 \Rightarrow \mu_p^{\text{anomalous}} \approx 1.792\, \mu_N \tag{26}$$

  - E704 at Fermilab used 200 GeV/c $\vec{p}$ from hyperon decay to detect asymmetry in scattering from H target [18]. Largest $A_y \approx 0.04$ with large statistical errors.
  - Meanwhile, accurate measurements of A_y are available from RHIC [19]
- Asymmetry measurements involve normalization uncertainties and calculations of A_y are subject to uncertainties in amplitudes of strong interaction. **Therefore, accurate calibration of reaction required.**

Coulomb-Nuclear interference II

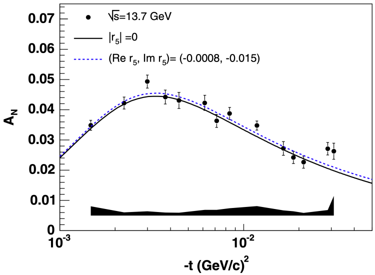

Measured A_N from RHIC in the CNI region at $\sqrt{s} = 6.8\,\text{GeV}$ ($E_\text{lab} = 23.7\,\text{GeV}$) [19].

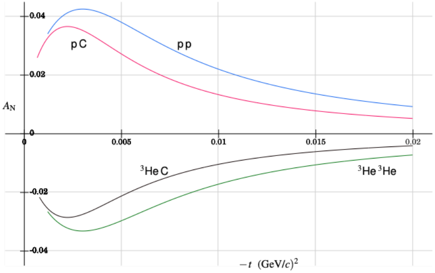

Calculation of A_y in the CNI region by Nigel Buttimore [20].

Critical field for hydrogen hyperfine splitting I

Zeeman region:

- magnetic flux density at which energy separation between different hyperfine levels becomes comparable to Zeeman splitting.
- referred to as *critical magnetic field* or *Breit-Rabi field* B_c
- Breit-Rabi formula (energy levels of hydrogen atom in external magnetic field:

$$E_{F,m_F} = -\frac{E_{\mathrm{hfs}}}{2(2I+1)} + g_J \mu_B m_J B \pm \frac{E_{\mathrm{hfs}}}{2}\sqrt{1 + \frac{2m_F x}{F} + x^2}\,, \text{where} \quad (27)$$

- E_{hfs} is hyperfine splitting energy
- I is nuclear spin (for H, $I = \frac{1}{2}$)
- g_J is Landé g-factor
- μ_B is Bohr magneton
- m_J is magnetic quantum number
- m_F is total angular momentum quantum number
- $x = \frac{g_J \mu_B B}{E_{\mathrm{hfs}}}$
- $F = I + J$ is total angular momentum (for H, $J = \frac{1}{2}$)

Critical field for hydrogen hyperfine splitting II

For H:

- hyperfine splitting energy $E_{\rm hfs}$ (1420 MHz):

$$E_{\rm hfs} \approx 5.874 \times 10^{-6}\,\mathrm{eV} \tag{28}$$

- Critical field B_c is when Zeeman energy $g_J \mu_B B$ is comparable to $E_{\rm hfs}$. With $g_J \mu_B B_c \approx E_{\rm hfs}$, we get:

$$B_c \approx \frac{E_{\rm hfs}}{g_J \mu_B} \tag{29}$$

- For H, $g_J \approx 2$ (approximately for electron), and $\mu_B \approx 5.788 \times 10^{-5}\,\mathrm{eV/T}$. Thus,

$$B_c \approx \frac{5.874 \times 10^{-6}\,\mathrm{eV}}{2 \times 5.788 \times 10^{-5}\,\mathrm{eV/T}} \approx 50.7\,\mathrm{mT} \tag{30}$$

Radiofrequency-fields

FFT of convolution

- Two-sided amplitude spectrum of FFT of the convolution

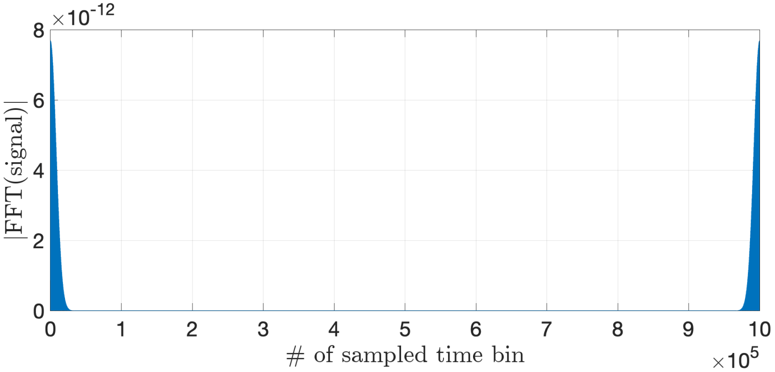

Amplitudes of magnetic RF fields

from FFT of convolution

- Same, but logy
- FFT background $\leq 1\%$
  - not at f_{rev}
  - not from finite set of δ fcts
  - $\rightarrow$ probably numerical from FFT

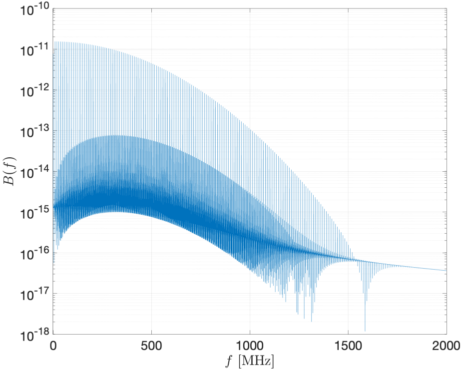

Will carbon fiber targets survive at EIC?

Target heating calculated according to Peter Thieberger

- With proper beam sizes, there is not much difference between RHIC and EIC.
- RF heating of the target supports not included, will be more severe at EIC due to shorter bunches.
- RF design of target holders needs to be optimized.

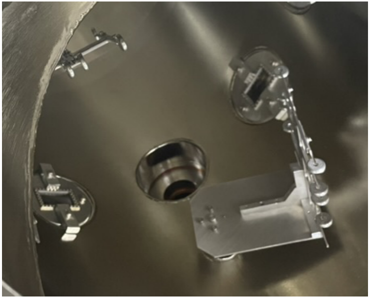

CNI polarimeter setup

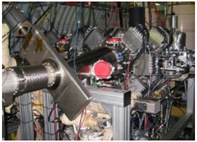

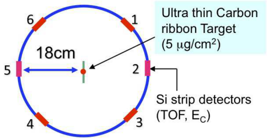

CNI setup with 6 Si detectors at different azimuth at each target enables

- determination of polarization components P_x and P_y
- determination of polarization profile along x and y
- Due to parity violation, $A_z \approx 0$ (no longitudinal analyzing power) $\rightarrow$ P_z not measurable with *unpolarized* target

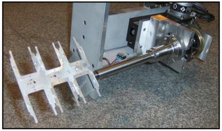

Ultra-thin ribbon targets

- 8 target holder inside beam pipe
- 2 holders per beam for x and y
- 6 targets per holders, 48 in total
- Targets $\approx 10\,\mu m \times 100\,nm$, hand crafted by D. Steski & team

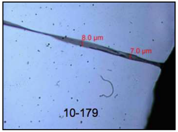

Carbon target temperatures from Thieberger's estimate

RHIC typical conditions

- 250 GeV
- 111 bunches
- 16×10^{10} protons per bunch
- $\sigma_r^{95} = 0.68\,\mathrm{mm}$ (slide 27)

TARGET	GRAPHITE	TUNGSTEN	CARBON
Density (g/cc)	2.26	19.3	2.26
LET (MeV cm^2/g)	1.76E-03	1.12E-03	6.33E-04
Thermal conductivity [W/(K * m)]	390	173	390
Emissivity	0.8	0.35	0.8
Specific heat (J/ (gm K)	0.72	0.134	0.72
Thickness (nm)	50	100	50
Sublimation or melting limit (°C)	2227	3422	2227

PROTON BEAM	RHIC 2017	EIC	XX bunch
Beam rms width (mm)	0.68	1.2	
# of protons per bunch	1.60E+11	6.90E+10	
# of bunches	111	1160	

Thermal conductivity multiplier	1
Simulation time step (ns)	500

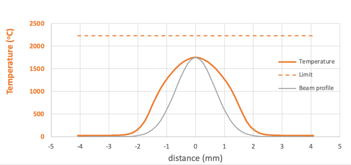

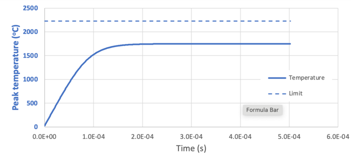

Carbon target temperatures from Thieberger's estimate

EIC for highest luminosity

- 275 GeV
- 1160 bunches
- 6.9×10^{10} protons per bunch
- $\sigma_r^{95} = 1.2\,\text{mm}$ **cooled beam**

TARGET	GRAPHITE	TUNGSTEN	CARBON
Density (g/cc)	2.26	19.3	2.26
LET (MeV cm^2/g)	1.76E-03	1.12E-03	6.33E-04
Thermal conductivity [W/(K * m)]	390	173	390
Emissivity	0.8	0.35	0.8
Specific heat (J/ (gm K)	0.72	0.134	0.72
Thickness (nm)	50	100	50
Sublimation or melting limit (°C)	2227	3422	2227

PROTON BEAM	RHIC 2017	EIC	XX bunch
Beam rms width (mm)	0.68	1.2	
# of protons per bunch	1.60E+11	6.90E+10	
# of bunches	111	1160	

Thermal conductivity multiplier	1
Simulation time step (ns)	500

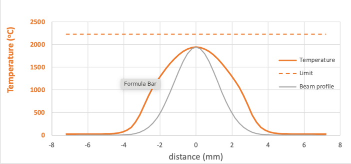

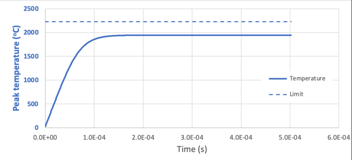

Carbon target temperatures from Thieberger's estimate

EIC for highest luminosity

- 275 GeV
- 1160 bunches
- 6.9×10^{10} protons per bunch
- $\sigma_r^{95} = 2.8\,\text{mm}$ **uncooled beam** (slide 30)

TARGET	GRAPHITE	TUNGSTEN	CARBON
Density (g/cc)	2.26	19.3	2.26
LET (MeV cm^2/g)	1.76E-03	1.12E-03	6.33E-04
Thermal conductivity [W/(K * m)]	390	173	390
Emissivity	0.8	0.35	0.8
Specific heat (J/ (gm K)	0.72	0.134	0.72
Thickness (nm)	50	100	50
Sublimation or melting limit (°C)	2227	3422	2227

PROTON BEAM	RHIC 2017	EIC	XX bunch
Beam rms width (mm)	0.68	2.8	
# of protons per bunch	1.60E+11	6.90E+10	
# of bunches	111	1160	

Thermal conductivity multiplier	1
Simulation time step (ns)	500

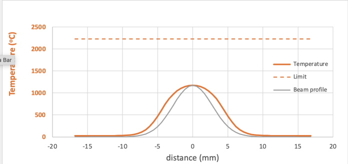

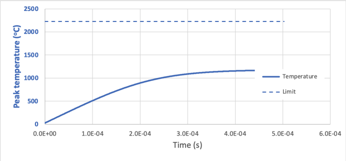

Direct measurement of temperature of carbon targets

Work with Vera Shmakova, Prashanth Shanmuganathan, Oleg Eyser, Haixin Huang, Dannie Steskie, Thomas Tsang, and George Mahler

- Carbon fiber targets of RHIC polarimeters do not reach carbon sublimation temperature of $T_{\text{sub}} = 3915\,\text{K}$: **targets survive proton bombardment**.
  - Observation aligns with energy loss calculations by Peter Thieberger (BNL) using appropriate beam sizes at the interaction point.
- Direct temperature measurement of carbon targets remains crucial goal
  - Black-body radiation [21] as a method to determine temperature by analyzing the emitted light spectrum.
- **APEX measurement approved for run 25**
  - more details on this investigations on slides slides 74 – 78

Experimental setup

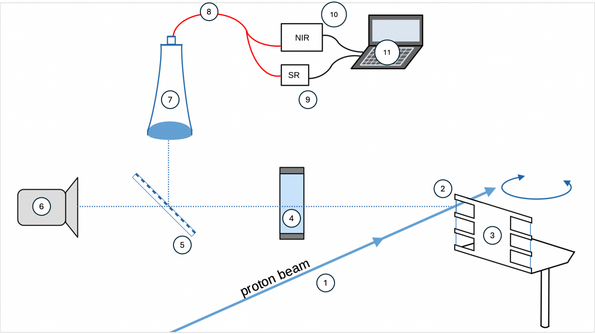

1. proton beam
2. fiber target
3. target holder
4. fused-silica viewport
5. semi-transparent polka-dot mirror
6. optical camera
7. collimator lens
8. fiber splitter (VIS and IR)
9. spectrometer VIS (SR)
10. spectrometer IR (NIR)
11. spectral analysis ($\lambda = 200 - 2200\,\mathrm{nm}$)

Black body radiation

Ideally, one would measure:

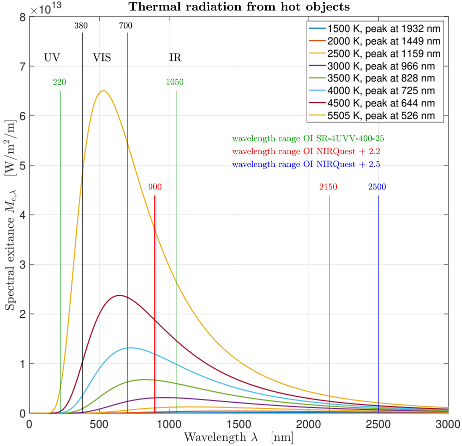

wavelength-dependent attenuation in

- fused-silica viewport
- collimator lens
- 100 m glass fibers from IP12 to spectrometers

Lab test measurement using IR light source

Experimental setup

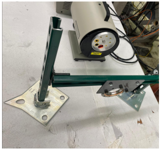

Black body radiation using oven at 1463 K

- SR spectrometer: 200 to 900 nm
- NIR spectrometer: 900 to 2100 nm
- Light path includes fiber splitter and 100 m glass fibers
- Measured spectrum compared to blackbody radiation spectra at 1463 K, 1263 K, and 1663 K

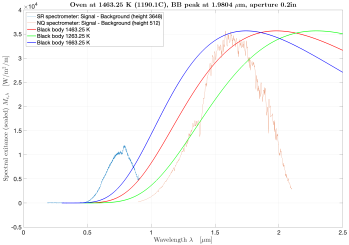

Test measurements using C targets at IP4

- In 2024, equipment/components arrived late, thus optimal alignment of light collection system at IP4 was not possible.
- We observe a clear signal, however, the light intensity is low because we don't aim at the brightest spot on the target
- For the same reason, the temperature we observe is only around 1400 K, about half of what we would expect

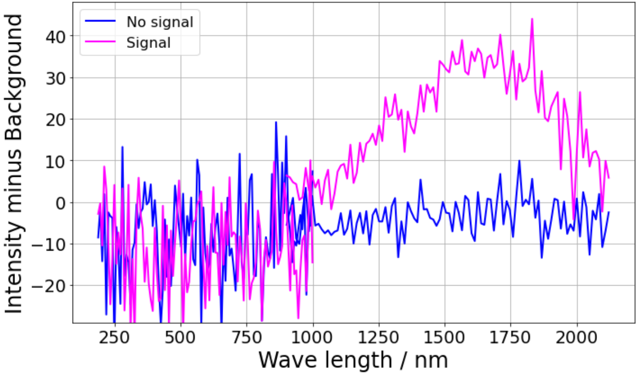

APEX proposal

Goals for run 25

- **Ensure full understanding of energy loss/heating of carbon polarimetry fiber targets by high energy proton beam, in particular for EIC**
- Light collection system was installed and operated already during run 24
  - As CNI chamber was already sealed off/pumped down when all components were available, light collection system could not be properly aligned
- **Improve alignment before ring closes, repeat measurement in run 25**
  1. Our APEX requires dedicated time only in case no proton beam available in run 25. With 100 GeV stored protons, we can run parasitically.
  2. Need 100 GeV protons in blue with max. number of bunches stored
  3. With beam on flattop, a single fill of the machine should be sufficient:
     - Sweep one target back and forth through the beam, then do another one, and so on. No need to wait for target cool down.
     - Will use four targets in blue, two horizontal ones and two vertical ones.
  4. 2h sweeping targets back and forth sufficient to achieve goals
  5. In case something goes wrong with 3. and 4., we need a 2nd fill